Int. J. Heat Mass Transfer. Vol. 26, No. 3, pp. 389 399, 1983
Printed in Great Britain

0017 9310/83/030389 11 $03.00/0
Pergamon Press Ltd.

A NEW HYDRODYNAMIC MODEL OF CRITICAL HEAT FLUX, APPLICABLE WIDELY TO BOTH POOL AND FORCED CONVECTION BOILING ON SUBMERGED BODIES IN SATURATED LIQUIDS

Y. HARAMURA and Y. KATTO
Department of Mechanical Engineering, University of Tokyo, Bunkyo-ku, Tokyo, Japan

(*Received* 23 *May* 1982)

Abstract—In this paper, Helmholtz instability is imposed on the vapor–liquid interface of columnar vapor stems distributed in a liquid layer wetting a heated surface. This vapor–liquid system is collapsed wholly by the instability, but due to the suppression of the solid surface, a thin liquid film including vapor stems is left stable on the surface with a certain definite thickness relating to the Helmholtz critical wavelength. A vapor blanket, thus formed on the liquid film, restricts the feed of liquid from the bulk region to the film, resulting in the disappearance of liquid from the heated surface, that is, the appearance of critical heat flux (CHF). Based on the foregoing concept, a new hydrodynamic model is developed, and analyses of CHF in fundamental boiling systems are exemplified not only for pool boiling but also for forced convection boiling, suggesting the validity of the physical structure of this model.

NOMENCLATURE

A_v, cross-sectional area of vapor stems [m^2];
A_w, area of heated surface [m^2];
d, diameter of cylinder or disk [m];
G, mass velocity of liquid, $u\rho_l$ [$kg\ m^{-2}\ s^{-1}$];
g, acceleration due to gravity [$m\ s^{-2}$];
H_{fg}, latent heat of evaporation [$J\ kg^{-1}$];
H, vertical dimension of horizontal ribbon [m];
H', dimensionless height, $H/[\sigma/g(\rho_l-\rho_v)]^{1/2}$;
k, factor for liquid addition due to inflow;
l, length of flat plate [m];
q, heat flux [$W\ m^{-2}$];
q_{c0}, critical heat flux in saturated boiling [$W\ m^{-2}$];
$q_{c0,Z}$, q_{c0}, predicted by Zuber's equation (1) [$W\ m^{-2}$];
R', dimensionless radius, $(d/2)/[\sigma/g(\rho_l-\rho_v)]^{1/2}$;
t, time [s];
u, velocity of uniform liquid flow [$m\ s^{-1}$];
u_l, velocity of liquid [$m\ s^{-1}$];
u_v, velocity of vapor [$m\ s^{-1}$];
v_1, volumetric growth rate of bubble [$m^3\ s^{-1}$].

Greek symbols
δ_c, critical thickness of liquid film [m];
λ, wavelength [m];
λ_c, Taylor critical wavelength [m];
λ_D, λ'_D, most susceptible (or dangerous) Taylor wavelength [m];
λ_H, Helmholtz critical wavelength [m];
ρ_l, density of liquid [$kg\ m^{-3}$];
ρ_v, density of vapor [$kg\ m^{-3}$];
σ, surface tension [$N\ m^{-1}$];
τ_d, hovering period of bubble [s].

1. INTRODUCTION

FOR CRITICAL heat flux in pool boiling, a number of models have been proposed, but the one that seems to have been most widely accepted is that presented by Zuber [1] for the boiling on an infinite, upward-facing, horizontal, flat plate [2]. This model postulates that the vapor generated at the flat plate accumulates to form a continuous columnar escape flow of diameter $\lambda_c/2$ at intervals of Taylor critical wavelength λ_c, and that CHF takes place when the vapor–liquid interface of the escape passage becomes unstable due to Helmholtz instability. However, the magnitude of the Helmholtz critical wavelength λ_H is indefinite, so it is determined as $\lambda_H = \pi\lambda_c/2$ from the Rayleigh stability limit of a circular gas jet in a liquid, and a few approximations such as $3/\sqrt{2\pi} \doteqdot 1$ are made to give the critical heat flux $q_{c0,Z}$ as

$$\frac{q_{c0,Z}}{\rho_v H_{fg}}\Big/\left[\frac{\sigma g(\rho_l-\rho_v)}{\rho_v^2}\right]^{1/4} = 0.131. \qquad (1)$$

As is well known, equation (1) has the same form as the older equation of Kutateladze [3] correlating experimental data through dimensional analysis.

Extending Zuber's model to include finite bodies such as illustrated in Fig. 1, Lienhard and co-workers [4–7] carried out a number of studies about CHF with many valuable results. Furthermore, Lienhard and others [8–11] attempted to explain CHF in forced convection boiling as well as in pool boiling, by replacing hydrodynamic instability analyses with a very simple concept of "mechanical energy stability criterion", which considers a balance between the kinetic energy of the vapor flow and the surface energy necessary to develop the vapor–liquid interface.

However, it must be noted that in the case of infinite plates, the vapor outflow and the incoming liquid flow become unstable simultaneously because of the counter flow pattern. This is not so in Fig. 1, where the incoming liquid flow can remain stable even if the vapor escape passage has collapsed. In addition, as Chang pointed out [12], the continuous vapor escape passages such as

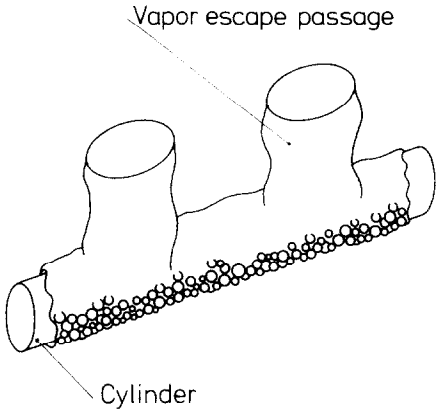

FIG. 1. Pool boiling at high heat fluxes on a horizontal cylinder.

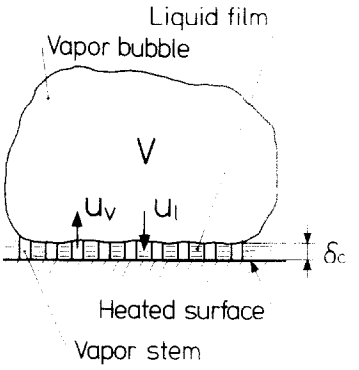

FIG. 2. Vapor structure near heated surface at high heat fluxes.

illustrated in Fig. 1, to which Helmholtz instability is applied, are quite different in nature from the actual flow aspects involving vapor slugs with unsteady-state behavior.

Meanwhile, for nucleate boiling at high heat fluxes, Gaertner and Westwater [13, 14] reported the following facts from the experiments of pool boiling of saturated water at atmospheric pressure: (i) as illustrated in Fig. 2, the heated surface is wetted with a liquid film, which includes numerous, continuous, columnar vapor stems, (ii) the massive vapor bubble, sitting on the liquid film and being nourished with vapor from the underlying vapor stems, rises away from the liquid film when it grows enough, and after a bubble leaves the liquid film, a new one is immediately established in its place, (iii) as for vapor stems, the population density increases while the diameter decreases as heat flux is increased, and the total cross-sectional area of vapor stems remains constant independently of heat flux, and (iv) the height to diameter ratio of vapor stem is kept constant independently of heat flux, which means that the height of vapor stem (thickness of liquid film) decreases with increasing heat flux.

For the massive vapor bubbles generated successively on the liquid film, the following quantitative behaviors have been reported by Katto and Yokoya [15]. First, the heat transferred constantly from the heated surface is absorbed by latent heat in the liquid film, and consequently the bubble volume V increases in proportion to the time t after the commencement of growth as

$$V = v_1 t \tag{2}$$

where v_1 is the volumetric growth rate of bubble. Second, the hovering* behavior of the massive bubble growing on the liquid film can be analyzed by utilizing the theory of Davidson and others [16, 17] for the periodic formation of bubble due to the flow of gas into a liquid, where the upward motion of a growing bubble is determined by a balance between the buoyancy force and the upward mass acceleration of the two-phase fluid. Thus, the hovering period for a bubble of volumetric growth rate v_1 is given as

$$\tau_d = \left(\frac{3}{4\pi}\right)^{1/5}\left[\frac{4(\xi\rho_l+\rho_v)}{g(\rho_l-\rho_v)}\right]^{3/5} v_1^{1/5}, \quad \xi = \tfrac{11}{16} \tag{3}$$

where ξ, the volumetric ratio of the accompanying liquid to the moving bubble, can be assumed to be 11/16 for the present purpose. Equations (2) and (3) can predict a relationship between the bubble formation frequency and the bubble diameter, agreeing well with the empirical relationship obtained by Ivey [18] from the data of high heat flux boiling [15].

In the present study, therefore, a new hydrodynamic model will be created so as to include not only Helmholtz instability effect but also the actual fluid behaviors such as mentioned above, and the validity of this model will be tested for forced convection boiling as well as for pool boiling.

2. A NEW HYDRODYNAMIC MODEL

2.1. *Thickness of liquid film* δ_c

Consider the case that the liquid film shown in Fig. 2 is sufficiently thick,† so the heat transferred from the heated surface is absorbed by latent heat near the base of vapor stems, inducing the upward vapor velocity u_v in the stems and the corresponding downward liquid velocity u_l. In this case, first, it is well known that the wave velocity c in the vapor–liquid interface of stems is given theoretically by

$$c = \pm\left[\frac{1}{\rho_l+\rho_v}\frac{2\pi\sigma}{\lambda} - \frac{\rho_l\rho_v}{(\rho_l+\rho_v)^2}(u_v+u_l)^2\right]^{1/2}. \tag{4}$$

Second, the heat balance $qA_w = \rho_v u_v A_v H_{fg}$ gives

$$u_v = (q/\rho_v H_{fg})/(A_v/A_w) \tag{5}$$

* This massive bubble hovers on the liquid film mainly due to the hydrodynamic action, because the surface tension of vapor stems is generally much weaker than the buoyancy force.

† The thickness of liquid film determined in this chapter will be used as the initial thickness (maximum value) of liquid film in the subsequent analyses of CHF.

where q is the heat flux, A_v the cross-sectional area of the vapor stems, and A_w the area of the heated surface. Third, the continuity equation $\rho_v u_v A_v = \rho_l u_l (A_w - A_v)$ gives

$$u_l/u_v = (\rho_v/\rho_l)(A_v/A_w)/[1-(A_v/A_w)]. \quad (6)$$

Equation (6) reveals that u_l/u_v is far less than unity, because $\rho_v/\rho_l < 1$, and also A_v/A_w is much less than unity as will be found in Section 2.3. Therefore, using u_v of equation (5), and ignoring u_l as compared with u_v, equation (4) with $c = 0$ gives the critical wavelength λ_H for Helmholtz instability as

$$\lambda_H = 2\pi\sigma \frac{\rho_l+\rho_v}{\rho_l\rho_v}\left(\frac{A_v}{A_w}\right)^2\left(\frac{\rho_v H_{fg}}{q}\right)^2. \quad (7)$$

However, we must not forget that the wave motion is suppressed by the solid surface, and its effect must extend to a certain distance from the surface. In other words, a liquid film including vapor stems (causes of instability) can exist stably up to the distance δ_c from the heated surface. The exact value of δ_c is unknown at the present time, but it must depend on the unstable wavelength, being probably somewhere between $\delta_c = 0$ and $\delta_c = \lambda_H/2$. In the present paper, therefore, δ_c is assumed tentatively to be the middle value:

$$\delta_c = (0+\lambda_H/2)/2 = \lambda_H/4,$$

when δ_c can be determined through equation (7) as follows

$$\delta_c = \frac{\lambda_H}{4} = \frac{\pi}{2}\sigma\frac{\rho_l+\rho_v}{\rho_l\rho_v}\left(\frac{A_v}{A_w}\right)^2\left(\frac{\rho_v H_{fg}}{q}\right)^2. \quad (8)$$

2.2. *CHF on a horizontal, infinite flat plate*

Equation (8) includes an unknown quantity A_v/A_w, but the CHF on an infinite, horizontal flat plate will be analyzed before proceeding to the evaluation of A_v/A_w, for the sake of convenience.

Figure 3 illustrates the configuration of the nucleate boiling on an infinite plate corresponding to Gaertner and Westwater's observations (i) and (ii) mentioned in Section 1. The interval λ_D between bubbles is determined by Taylor instability, and according to the studies of Lienhard and others [7, 4], we must take the most susceptible (or dangerous) wavelength instead of critical wavelength, thus

$$\lambda_D = 3^{1/2}2\pi[\sigma/g(\rho_l-\rho_v)]^{1/2}. \quad (9)$$

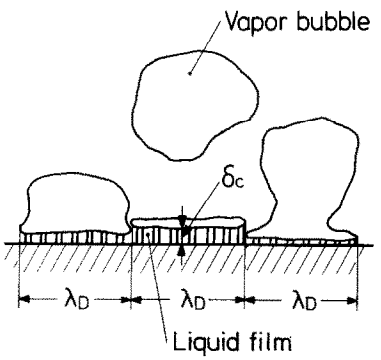

FIG. 3. Pool boiling at high heat fluxes on a horizontal, infinite flat plate.

Now, the unit heater area participating in the growth of one vapor bubble is λ_D^2 [19, 20], and therefore, if the heat flux is q, the volumetric growth rate of bubble v_l in equation (2) is given as

$$v_l = \lambda_D^2 q/(\rho_v H_{fg}) \quad (10)$$

and the corresponding hovering time of bubble τ_d is given by equation (3).

Now, if the liquid film on the heated surface is not fed with liquid from the bulk region during the hovering period of bubble τ_d, then it can be postulated that CHF appears when the liquid film evaporates away at the end of the hovering time, for which the heat balance is written as

$$\tau_d q A_w = \rho_l \delta_c (A_w - A_v) H_{fg} \quad (11)$$

where δ_c is the initial thickness of the liquid film at the start of bubble growth, and it has been given by equation (8). Thus, solving equations (2), (3) and (8)–(11) for the critical heat flux q, and writing q as $q_{c0,Z}$ gives

$$\frac{q_{c0,Z}}{\rho_v H_{fg}}\Bigg/\left[\frac{\sigma g(\rho_l-\rho_v)}{\rho_v^2}\right]^{1/4} = \left(\frac{\pi^4}{2^{11}\cdot 3^2}\right)^{1/16}\left(\frac{A_v}{A_w}\right)^{5/8}\left(1-\frac{A_v}{A_w}\right)^{5/16} \times\left[\left(\frac{\rho_l}{\rho_v}+1\right)\Bigg/\left(\frac{11}{16}\frac{\rho_l}{\rho_v}+1\right)^{3/5}\right]^{5/16}. \quad (12)$$

2.3. *Evaluation of* A_v/A_w

For Zuber's model described at the beginning of Section 1, Lienhard *et al.* [6] advocate that the interval λ_c between the escape passages should be λ_D of equation (9), and that Helmholtz unstable wavelength λ_H determined as $\lambda_H = \lambda_D$ is preferable to Zuber's $\lambda_H = \pi\lambda_c/2$, resulting in the increase of the constant on the RHS of equation (1) by 14%. Examining the data of critical heat flux q_{c0} obtained for finite, horizontal, flat plates with vertical side walls to prevent induced convection effect (i.e. to simulate the condition of infinite plates), Lienhard *et al.* regarded the foregoing result of $q_{c0}/q_{c0,Z} = 1.14$ as appropriate. However, the data points of $q_{c0}/q_{c0,Z}$ plotted in Fig. 8 of ref. [6] are statistically somewhat below 1.14 in the range of $L/\lambda_D > 3$, where L is the representative length of the finite plate. Also, the data listed in Table 1 of ref. [6] give average $q_{c0}/q_{c0,Z} = 1.07$ for $L/\lambda_D > 3$, and average $q_{c0}/q_{c0,Z} = 1.06$ for $L/\lambda_D > 9.8$. In the present paper, therefore, it will be assumed, for simplification purposes, that Zuber's original equation (1) applies to the CHF of infinite flat plates.

Now, we can postulate that the RHS of equation (12) equals that of equation (1), and if the assumption of

$A_v/A_w \ll 1$ in Section 2.1 is used again, it yields

$$\frac{A_v}{A_w} = 0.0654\left[\left(\frac{11}{16}\frac{\rho_l}{\rho_v}+1\right)^{3/5}\Big/\left(\frac{\rho_l}{\rho_v}+1\right)\right]^{1/2}. \quad (13)$$

For $\rho_v/\rho_l \ll 1$, equation (13) can be reduced to

$$A_v/A_w = 0.0584(\rho_v/\rho_l)^{0.2}. \quad (14)$$

The values of A_v/A_w calculated by equations (13) and (14) are compared in Fig. 4, suggesting that equation (14) will be enough to predict A_v/A_w up to $\rho_v/\rho_l = 1$ if only minor errors are ignored near $\rho_v/\rho_l = 1$. Equation (14) is in accord with Gaertner and Westwater's observation (iii) mentioned in Section 1, that A_v/A_w is kept constant independently of q for fixed ρ_v/ρ_l. In addition, Fig. 4 shows that the magnitude of A_v/A_w is rather unchangeable, and is much less than unity. This explains well the empirical fact that when wetted with a liquid film, the heated surface is cooled in spite of the existence of numerous vapor stems in the liquid film. Substituting A_v/A_w of equation (14) into the RHS of equation (5) gives

$$u_v = 17.1(q/\rho_v H_{fg})/(\rho_v/\rho_l)^{0.2}.$$

For water boiling at atmospheric pressure and at the critical heat flux q as given by equation (1), the above equation predicts $u_v = 61.5\,\mathrm{m\,s^{-1}}$. If compared with the sonic velocity of steam 473.5 m s^{-1} at 0.1 MPa and 100°C, the value of 61.5 m s^{-1} is relatively very low (Mach number 0.13), suggesting that there are no serious problems associated with sonic velocity.

Finally, the thickness of liquid film δ_e can be determined by substituting A_v/A_w of equation (14) into the RHS of equation (8) as follows:

$$\frac{\delta_e(q/H_{fg})^2}{\sigma\rho_v} = 0.00536\left(\frac{\rho_v}{\rho_l}\right)^{0.4}\left(1+\frac{\rho_v}{\rho_l}\right). \quad (15)$$

Equation (15) predicts a character that δ_e varies in proportion to $1/q^2$ under the condition of fixed pressure, which accords with Gaertner and Westwater's observation (iv) mentioned in Section 1. For water boiling at atmospheric pressure with a heat flux of $q = 0.946\ \mathrm{MW\,m^{-2}}$, equation (15) predicts $\delta_e = 0.056$ mm, while Gaertner [14] measured the average height of vapor stems as $\delta_e = 0.12$ mm at the periphery of a horizontal 50.8 mm dia. disk heater. The measured δ_e is about twice as thick as the predicted δ_e, but the liquid film must have a greater thickness in the peripheral region than in the interior, because of the straightforward exposure to the bulk liquid. Therefore, the assumption of $\delta_e = \lambda_H/4$ for the relationship between δ_e and λ_H made in Section 2.1 will be left as it is.

3. CHF FROM FINITE BODIES IN POOL BOILING

In order to test the validity of the model derived in Section 2, a few typical analyses of CHF in pool boiling will be made.

3.1. *Infinitely long, horizontal cylinder*

The configuration of high heat flux boiling on an infinitely long, horizontal cylinder of a comparatively small diameter d (actually, the length to diameter ratio must be greater than, say, 20) is shown in Fig. 5(a). In this case, a liquid film of thickness δ_e including vapor stems appears on the cylindrical surface as illustrated in Fig. 5(b). Thus, the heat balance associated with the total evaporation of a liquid film in an hovering period of bubble τ_d is given by the following equation, instead of equation (11),

$$\tau_d q A_w = \rho_l \delta_e (A_w - A_v + A_w \delta_e/d) H_{fg}. \quad (16)$$

But, excluding the case of excessively small diameter, the normal condition of cylinder will be considered below, where δ_e/d is far less than unity, and hence the third term in the parentheses on the RHS of equation (16) can be ignored as compared with the first term.

According to the study of Lienhard and Wong [7], the most susceptible wavelength λ_D' for the horizontal, cylindrical vapor–liquid interface is given by the following equation, instead of equation (9), due to the additional effect of surface tension along the curvature

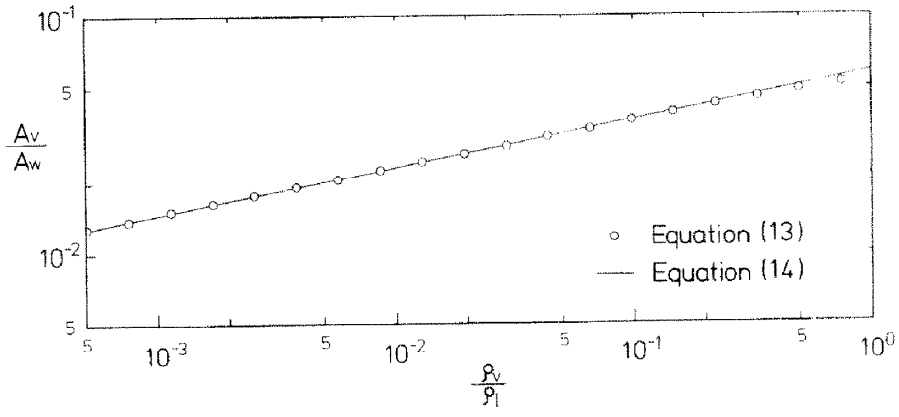

FIG. 4. Magnitude of A_v/A_w.

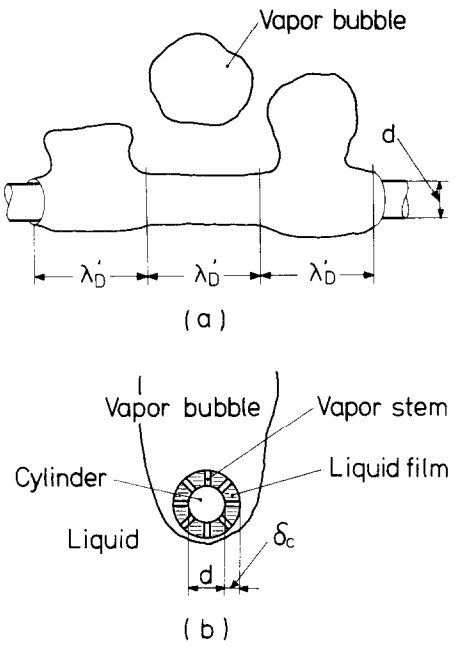

FIG. 5. Pool boiling at high heat fluxes on a horizontal cylinder.

in the transverse direction:

$$\lambda_D' = 3^{1/2} \cdot 2\pi \left\{ \frac{\sigma}{g(\rho_l - \rho_v)} \Big/ \left[1 + \frac{2\sigma}{d^2 g(\rho_l - \rho_v)} \right] \right\}^{1/2}. \quad (17)$$

Since the unit heater area participating to the growth of one vapor bubble is now $\pi d\lambda_D'$ as is noticed from Fig. 5(a), the volumetric growth rate of bubble v_1 is

$$v_1 = \pi d \lambda_D' q / (\rho_v H_{fg}). \quad (18)$$

Thus, solving equations (2), (3), (8) and (16)–(18) for q under the above-mentioned condition of $\delta_c/d \ll 1$, and writing the q as q_{c0} result in

$$\frac{q_{c0}}{\rho_v H_{fg}} \Big/ \left[\frac{\sigma g(\rho_l - \rho_v)}{\rho_v^2} \right]^{1/4} = \left(\frac{\pi^4}{2^{11} \cdot 3^2} \right)^{1/16} \left(\frac{A_v}{A_w} \right)^{5/8} \left(1 - \frac{A_v}{A_w} \right)^{5/16} \times \left[\left(\frac{\rho_l}{\rho_v} + 1 \right) \Big/ \left(\frac{11}{16} \frac{\rho_l}{\rho_v} + 1 \right)^{3/5} \right]^{5/16} \times \left(\frac{\sqrt{3}}{R'} \right)^{1/16} \left[1 + \frac{1}{2(R')^2} \right]^{1/32} \quad (19)$$

where $R' = (d/2)/[\sigma/g(\rho_l - \rho_v)]^{1/2}$. Comparison of equation (19) for cylinders with equation (12) for infinite plates gives the following relation:

$$\frac{q_{c0}}{q_{c0,Z}} = \left(\frac{\sqrt{3}}{R'} \right)^{1/16} \left[1 + \frac{1}{2(R')^2} \right]^{1/32} \quad (20)$$

where the value of $q_{c0,Z}$ is given by Zuber's equation (1).

In Fig. 6, the value predicted by equation (20) is compared with the range of about 900 experimental data points collected by Sun and Lienhard [5], and shows a fairly good agreement. For caution's sake, it is noted that if all the terms on the RHS of equation (16) are taken into account along with the conditions that A_v/A_w is given by equation (14) and $A_v/A_w \ll 1$, then the following equation is derived instead of equation (20):

$$\frac{q_{c0}}{q_{c0,Z}} = \left(\frac{\sqrt{3}}{R'} \right)^{1/16} \left[1 + \frac{1}{2(R')^2} \right]^{1/32} \times \left[1 + 0.156 \left(\frac{\rho_v}{\rho_l} \right)^{0.4} \left(1 + \frac{\rho_v}{\rho_l} \right) \frac{1}{R'(q_{c0}/q_{c0,Z})^2} \right]^{5/16}. \quad (20a)$$

Values of $q_{c0}/q_{c0,Z}$ predicted by equation (20) are compared with those of equation (20a) in Table 1, suggesting that with decreasing R', some slight

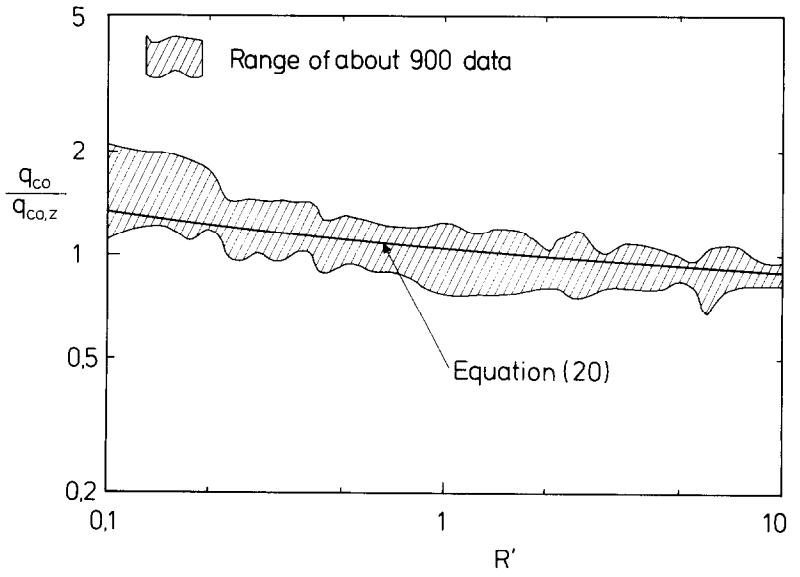

FIG. 6. Critical heat flux in pool boiling for horizontal cylinders.

Table 1. Values of $q_{co}/q_{co,z}$ predicted by equations (20) and (20a)

R'		0.1	0.2	0.5	1.0	10
$q_{co}/q_{co,z}$ by equation (20)		1.351	1.241	1.118	1.048	0.896
$q_{co}/q_{co,z}$ by equation (20a)	$\rho_v/\rho_l = 0.0001$	1.360	1.246	1.120	1.049	0.896
	$\rho_v/\rho_l = 0.001$	1.373	1.253	1.123	1.051	0.896
	$\rho_v/\rho_l = 0.01$	1.402	1.270	1.131	1.055	0.897
	$\rho_v/\rho_l = 0.1$	1.472	1.313	1.153	1.067	0.898
	$\rho_v/\rho_l = 1.0$	1.699	1.470	1.243	1.123	0.906

dispersions appear according to the change of ρ_v/ρ_l, particularly when R' is near 0.1 and ρ_v/ρ_l is very high.

3.2. *Infinitely long, horizontal ribbon oriented vertically*

Consider next the case of an infinitely long, horizontal, thin and flat ribbon heater with the broad side oriented vertically and with both sides heated. At the present time, the exact value of the most susceptible wavelength for Taylor instability is unknown. However, if the vertical dimension H of horizontal ribbon is sufficiently small, a rough estimation of CHF may possibly be made by substituting a cylinder of equal heated surface area for the ribbon. Various effects of the thickness of ribbon are now ignored for simplification purposes. Thus, the equivalent diameter d, defined by

$$\pi d = 2H \tag{21}$$

is substituted into equation (20) to give

$$\frac{q_{co}}{q_{co,z}} = \left(\frac{\sqrt{3}\pi}{H'}\right)^{1/16}\left[1+\frac{1}{2}\left(\frac{\pi}{H'}\right)^2\right]^{1/32} \tag{22}$$

where $H' = H/[\sigma/g(\rho_l-\rho_v)]^{1/2}$. Figure 7 shows a comparison of the value predicted by equation (22) with the experimental data listed in Table 1 of Lienhard and Dhir's paper [4]. Agreement is not so good as in Fig. 6, but it seems rather natural because of the use of various broad approximations.

3.3. *Upward-facing horizontal small disk*

When the diameter d of an upward-facing horizontal disk is much smaller than the most susceptible wavelength λ_D of Taylor instability, one vapor bubble is formed successively on the disk as illustrated in Fig. 8. In this case, the heated surface area for the formation of one bubble is $\pi d^2/4$, independent of λ_D, and the volumetric growth rate of bubble v_1 is

$$v_1 = (\pi d^2/4)q/(\rho_v H_{fg}). \tag{23}$$

Furthermore, it must be noted that in the preceding cases of Figs. 3 and 5, the inflow of liquid across the periphery of the base of a bubble is blocked up by adjoining vapor bubbles, but now the whole periphery of a small disk is exposed straightforwardly to the bulk liquid as seen in Fig. 8. Besides, according to the experimental study of Katto and Kikuchi [21], the vapor pressure within the bubble, averaged for a hovering period, is lower than the surrounding liquid pressure at the disk heater level due to the buoyant effect. Therefore, an inflow of liquid to the liquid film from the surrounding can take place even in the hovering period of bubble. Hence, in order to take the inflow effect into account, equation (11) is now modified as follows:

$$\tau_d q A_w = \rho_l \delta_c (A_w - A_v)(1+k) H_{fg} \tag{24}$$

where k is the factor for the liquid addition due to inflow. Katto and Kunihiro [22] have shown that CHF in pool boiling can be raised by artificial addition of liquid to the disk heater through a very thin tube. Hence, equations (2), (3), (8), (23) and (24) are solved for the critical heat flux q_{co}, and the comparison of q_{co} with

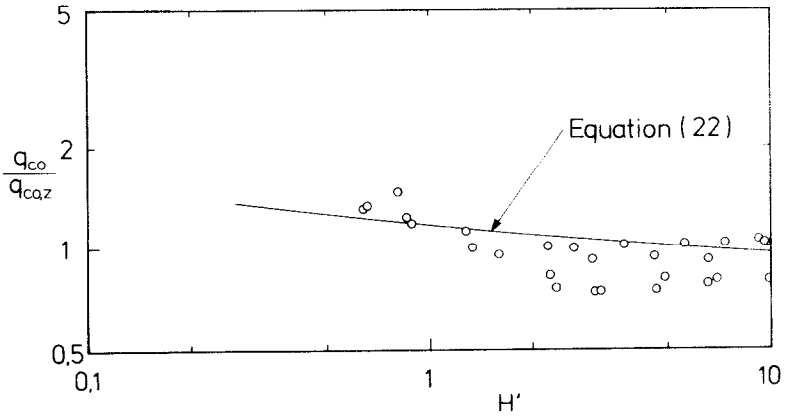

FIG. 7. Critical heat flux in pool boiling for horizontal ribbons oriented vertically.

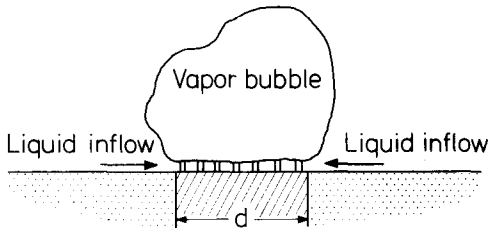

FIG. 8. Pool boiling at high heat fluxes on a horizontal disk.

$q_{c0,Z}$ of equation (12) gives

$$\frac{q_{c0}}{q_{c0,Z}} = (1+k)^{5/16} \times \left\{\left[3^{1/2}\cdot 2\pi\left(\frac{\sigma}{g(\rho_l-\rho_v)}\right)^{1/2}\right]^2 \Big/ \left(\frac{\pi}{4}d^2\right)\right\}^{1/16}. \quad (25)$$

Now, six q_{c0} data points (1.62, 1.70, 1.43, 1.30, 1.54 and 1.67 MW m^{-2}) found in previous studies [15, 23, 24] for saturated water boiling on a 10 mm dia. copper disk heater at atmospheric pressure are averaged to give $q_{c0} = 1.54$ MW m^{-2}, for which k in equation (25) is evaluated as $k = 0.83$. This is only an empirical value, but this value does not seem unreasonable for a small 10 mm dia. disk surrounded by the bulk liquid.

4. CHF IN FORCED CONVECTION BOILING OF EXTERNAL FLOW TYPE

Now, the model derived in Section 2 will be applied to the CHF in forced convection boiling on flat plates and cylinders submerged in saturated liquids flowing with sufficiently high velocities.

4.1. *Flat plates in a parallel flow*

Figure 9(a) illustrates nucleate boiling at high heat fluxes on a flat surface of length l parallel to a saturated liquid flow of velocity u. In this case, the vapor flowing out of numerous vapor stems distributed in a liquid film maintains a continuous vapor flow blanketing the liquid film. The underlying liquid film also forms a flow along the heated surface, decreasing its thickness in the direction of flow due to evaporation. Phenomena such as entrainment and deposition of droplets are ignored here, because they are presumed to be scarce. At the upstream end of the heated surface, the liquid film has a maximum thickness δ_c given by equation (15), and thereby can receive fresh liquid constantly from the main flow of velocity of u. Thus, it can be assumed that CHF appears when the heat being transferred from the heated surface of length l just balances with latent heat of the total evaporation of the liquid flowing into the liquid film.* Hence, the heat balance is written as

$$ql = \rho_l \delta_c u H_{fg}. \quad (26)$$

Substituting δ_c of equation (15) into equation (26), and writing q as q_{c0} gives

$$\frac{q_{c0}}{GH_{fg}} = 0.175\left(\frac{\rho_v}{\rho_l}\right)^{0.467}\left(1+\frac{\rho_v}{\rho_l}\right)^{1/3}\left(\frac{\sigma\rho_l}{G^2 l}\right)^{1/3} \quad (27)$$

where $G = u\rho_l$, the mass velocity of liquid flow. When ρ_v/ρ_l is much less than unity, equation (27) is reduced to

$$\frac{q_{c0}}{GH_{fg}} = 0.175\left(\frac{\rho_v}{\rho_l}\right)^{0.467}\left(\frac{\sigma\rho_l}{G^2 l}\right)^{1/3}. \quad (28)$$

Figure 10 shows a comparison of the values predicted by equation (28) with the experimental data obtained by Katto and Kurata [25] for water ($\rho_v/\rho_l = 0.000624$) and R-113 ($\rho_v/\rho_l = 0.00488$) flowing over the heated surfaces of $l = 10$, 15 and 20 mm at atmospheric

* This gives the answer to the question why the viscosity of fluid exerts no significant influences on the CHF in the forced convection boiling of external flow type.

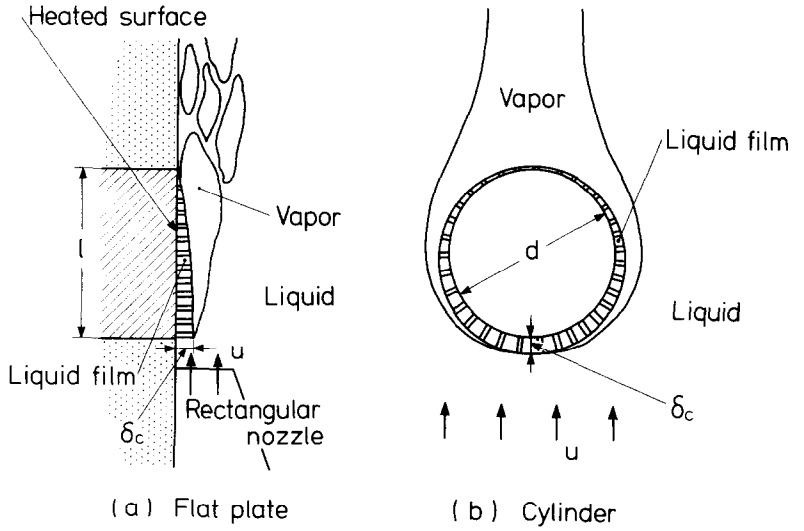

FIG. 9. Forced convection boiling at high heat fluxes. (a) A flat plate in a parallel flow, (b) a cylinder in a cross flow.

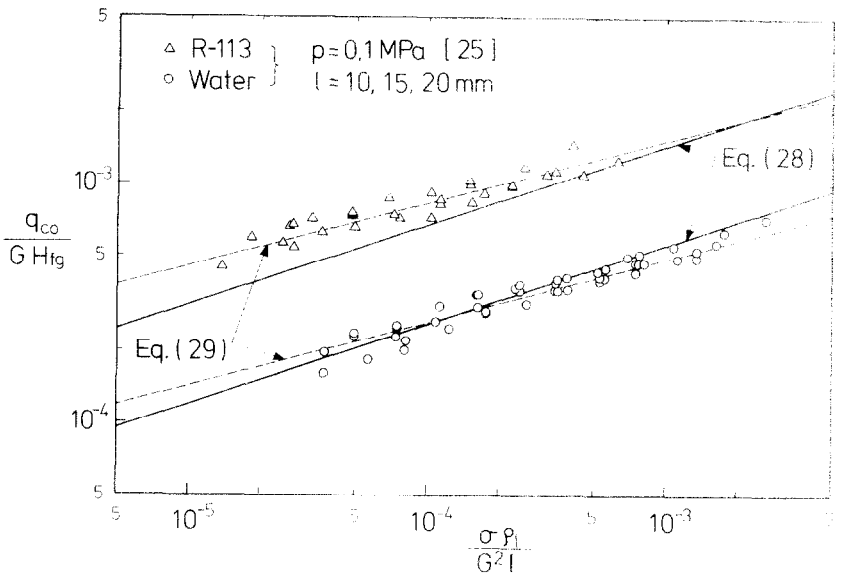

FIG. 10. Critical heat flux for flat plates in a parallel flow.

pressure. In Fig. 10 are also shown two broken lines representing the empirical equation obtained by Katto and Kurata for the above-mentioned data

$$\frac{q_{c0}}{GH_{fg}} = 0.186\left(\frac{\rho_v}{\rho_l}\right)^{0.559}\left(\frac{\sigma\rho_l}{G^2 l}\right)^{0.264}. \quad (29)$$

Agreement between the theoretical prediction and the experimental data points is fairly good for water, while it is somewhat inferior for R-113, though for unknown reasons at the present time. In any case, however, it can be noted from equation (29) and Fig. 10 that the experimental data points of both water and R-113 have the exponent of $\sigma\rho_l/G^2 l$ of about 0.26, which is slightly less than the theoretical value of 1/3 in equation (28). This difference may be attributable to the effects of forced flow on the flow conditions at the upstream end of the heated surface, such as the thickness of liquid film, the inflow of liquid, and some others.

4.2. *Cylinders in a cross flow*

Figure 9(b) illustrates nucleate boiling at high heat fluxes on a heated cylinder of diameter d perpendicular to a saturated liquid flow of velocity u. In this case, if the effect of curvature can be neglected, and if the same mechanism of CHF as in the preceding section can be assumed, then the flow structure along the semicircular surface extending from the front to the rear stagnation point becomes equivalent to that along a flat plate of the same length as the semicircle. Hence, putting $l = \pi d/2$ in equation (27) yields q_{c0} for a cylinder as follows:

$$\frac{q_{c0}}{GH_{fg}} = 0.151\left(\frac{\rho_v}{\rho_l}\right)^{0.467}\left(\frac{\sigma\rho_l}{G^2 d}\right)^{1/3}. \quad (30)$$

Figure 11 shows a comparison of the values predicted by equation (30) with the experimental data of water (symbol ○) and R-113 (symbol ×), both measured at atmospheric pressure: the former being the data of Vliet and Leppert [26, 27] for a comparatively small diameter $d = 3.18$ mm, the latter those of Yilmaz and Westwater [28] for $d = 6.5$ mm. It is interesting to note from Fig. 11 that like the case of flat plates shown in Fig. 10, the exponent of $\sigma\rho_l/G^2 d$ is nearly 0.26 for the data points of both water and R-113 (Yilmaz and Westwater [28] have given a relationship $q_{c0}/GH_{fg} = \text{const.}\,(\sigma\rho_l/G^2 d)^{0.26}$ to their data), suggesting the possibility of quite the same mechanism of CHF between the plate and the cylinder. The reason why the agreement between equation (30) and the data is inferior in the upper diagram of Fig. 11 may possibly be due to the effect of the curvature.

Meanwhile, broken lines in Fig. 11 represent the values predicted by the following equation obtained by Lienhard and Eichhorn [9] from the experimental data for four different kinds of fluids ($\rho_v/\rho_l = 0.00068$ to 0.0059 and $d = 0.5$ to 1.7 mm):

$$\frac{q_{c0}}{GH_{fg}} = \frac{1}{\pi}\left[\frac{1}{169}\left(\frac{\rho_v}{\rho_l}\right)^{1/4} + \frac{1}{19.2}\left(\frac{\rho_v}{\rho_l}\right)^{1/6}\left(\frac{\sigma\rho_l}{G^2 d}\right)^{1/3}\right]. \quad (31)$$

In the lower diagram of Fig. 11, the accuracy of equation (31) is clearly seen to be lost, and it is due to the specific character of equation (31) that q_{c0}/GH_{fg} tends to become constant with decreasing $\sigma\rho_l/G^2 d$ for fixed ρ_v/ρ_l. In the case of the upper diagram of Fig. 11, $\sigma\rho_l/G^2 d$ is on favorable orders, and hence the first term on the RHS of equation (31) can exert its proper effect on the second term. It must be noted here that equation (31) was derived by Lienhard and Eichhorn from the experimental data of $\sigma\rho_l/G^2 d$ ranging from 9×10^{-3} to 5×10^{-1}.

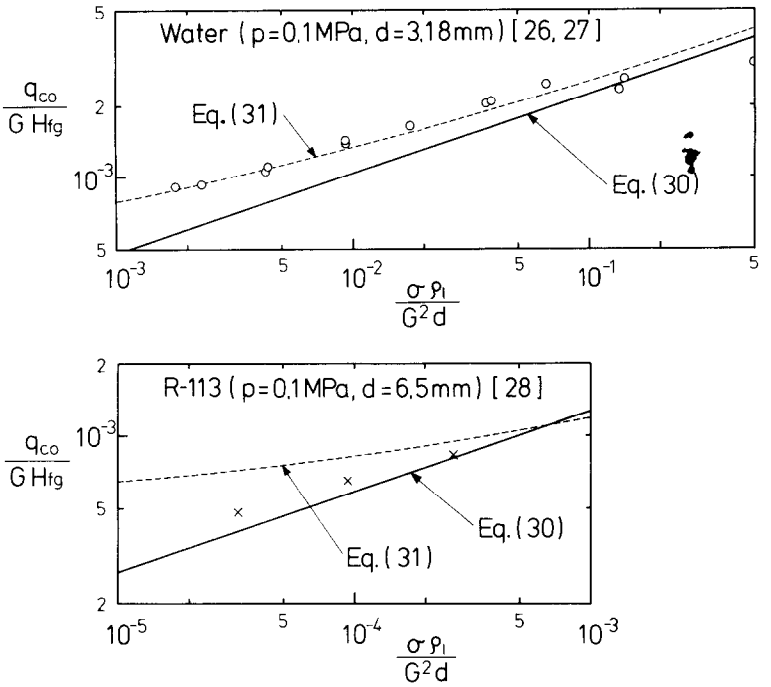

FIG. 11. Critical heat flux for cylinders in a cross flow.

5. MECHANISM TO APPROACH CHF IN NUCLEATE BOILING

It is well known [12, 14, 29] that nucleate boiling consists of two main regions : one is the 'isolated bubble' region at low heat fluxes, where a sequence of incipient discrete bubbles is maintained, and the other is the 'interference' region at high heat fluxes, where vapor structure such as illustrated in Fig. 2 appears on the heated surface. Hence, in view of the function of Helmholtz instability assumed in Section 2.1, we are led to a logical conclusion that throughout the interference region, nucleate boiling is subject to Helmholtz instability, maintaining the boiling configuration of Fig. 2 up to the CHF point. In other words, the interference region is nothing but the prodrome of CHF created by Helmholtz instability. This view is quite different from that of the existing instability model, where Helmholtz instability is assumed to act as the CHF point only, causing a sudden collapse of the vapor removal.

Besides, in the interference region mentioned above, the massive vapor blanket obstructs the feed of liquid from the bulk region. Therefore, the way the heated surface is fed with liquid ranks with Helmholtz instability in the importance for CHF. In pool boiling, the feed of liquid is performed through the periodical departure of the blanketing vapor bubble (Taylor instability relates to the bubble spacing only), and at times, there are the cases where the addition of liquid takes place due to the inflow of liquid across the periphery of the heated surface. In forced convection boiling, there is a steady-state flow of liquid into the liquid film at the upstream end of the heated surface.

As is well known, existing models of CHF are divided broadly into two opposite groups : one laying emphasis on the breakup of the vapor escape route due to hydrodynamic instability, and the other laying emphasis on the blockage of the liquid inflow due to vapor blanketing. Now, it is interesting to note that the new hydrodynamic model presented in this study is successful in making a compromise between the above two opposing groups, and moreover in overcoming difficulties in bridging the gap between pool and forced convection boiling. As to the mechanism with which transition boiling is introduced naturally after CHF, the description will be omitted here because it has been explained in a previous study [23] though in an imperfect form.

6. CONCLUSIONS

(1) Helmholtz instability originates the 'interference' region in nucleate boiling, leaving a stable liquid film of a certain definite thickness on the heated surface. CHF occurs through the total evaporation of liquid on the heated surface being subject to the restriction of the feed of liquid to the liquid film due to the vapor blanketing.

(2) Based on the physical structure mentioned above, a new hydrodynamic model has been developed, opening a sure access to CHF for various conditions of the heated surface and the fluid flow. A few examples of typical analyses of CHF have been shown in this paper not only for pool boiling but also for forced convection boiling on submerged bodies in saturated liquids, suggesting the broad validity of the model.

(3) As have been described in Section 5, the feed of liquid to the heated surface is no less important than

Helmholtz instability in the problem of CHF. Besides, in relation to the inflow of liquid, there are second scale problems proper to individual conditions, such as the liquid addition due to the inflow of liquid in pool boiling (Section 3.3), the effects of forced flow on the inflow conditions in forced convection boiling (Section 4), and others.

(4) In this paper, the heated surface is assumed to be wettable. In the case of very poor wettability, adequate modification must be made on the behavior of the liquid film on the heated surface.

Acknowledgement The support for this work provided by the Ministry of Education, Science and Culture: Special Project Research on Energy, Grant No. 57040016 (1982) is gratefully acknowledged.

REFERENCES

1. N. Zuber, Hydrodynamic aspects of boiling heat transfer, AEC Report No. AECU-4439 (1959).
2. G. F. Hewitt, Burnout, in *Handbook of Multiphase Systems* (edited by G. Hetsroni), pp. 6.109–6.122. Hemisphere, Washington (1976).
3. S. S. Kutateladze, A hydrodynamic model of the critical heat transfer in boiling liquids with free convection, *Zhurn. Tekhc. Fiz.* **20**(11), 1389–1392 (1950).
4. J. H. Lienhard and V. K. Dhir, Hydrodynamic prediction of peak pool-boiling heat fluxes from finite bodies, *Trans. Am. Soc. Mech. Engrs*, Series C, *J. Heat Transfer* **95**, 152–158 (1973).
5. K. H. Sun and J. H. Lienhard, The peak pool boiling heat flux on horizontal cylinders, *Int. J. Heat Mass Transfer* **13**, 1425–1439 (1970).
6. J. H. Lienhard, V. K. Dhir and D. M. Riherd, Peak pool boiling heat-flux measurements on finite horizontal flat plates, *Trans. Am. Soc. Mech. Engrs*, Series C, *J. Heat Transfer* **95**, 477–482 (1973).
7. J. H. Lienhard and P. T. Y. Wong, The dominant unstable wavelength and minimum heat flux during film boiling on a horizontal cylinder, *Trans. Am. Soc. Mech. Engrs*, Series C, *J. Heat Transfer* **86**, 220–226 (1964).
8. J. H. Lienhard and M. Z. Hasan, Correlation of burnout data for disk heaters cooled by liquid jets, *Trans. Am. Soc. Mech. Engrs*, Series C, *J. Heat Transfer* **101**, 383–384 (1979).
9. J. H. Lienhard and R. Eichhorn, On predicting boiling burnout for heater cooled by liquid jets, *Int. J. Heat Mass Transfer* **22**, 774–776 (1979).
10. J. H. Lienhard and R. Eichhorn, Peak boiling heat flux on cylinders in a cross flow, *Int. J. Heat Mass Transfer* **19**, 1135–1142 (1976).
11. J. H. Lienhard and M. Z. Hasan, On predicting boiling burnout with the mechanical energy stability criterion, *Trans. Am. Soc. Mech. Engrs*, Series C, *J. Heat Transfer* **101**, 276–279 (1979).
12. R. Moissis and P. J. Berenson, On the hydrodynamic transitions in nucleate boiling, *Trans. Am. Soc. Mech. Engrs*, Series C, *J. Heat Transfer* **85**, 221–229 (1963).
13. R. F. Gaertner and J. W. Westwater, Population of active sites in nucleate boiling heat transfer, *Chem. Engng Prog. Symp. Ser.* **56**(30), 39–48 (1960).
14. R. F. Gaertner, Photographic study of nucleate pool boiling on a horizontal surface, *Trans. Am. Soc. Mech. Engrs*, Series C, *J. Heat Transfer* **87**, 17–29 (1965).
15. Y. Katto and S. Yokoya, Behavior of a vapor mass in saturated nucleate and transition pool boiling, *Heat Transfer – Japan. Res.* **5**(2), 45–65 (1976).
16. J. F. Davidson and B. O. G. Schueler, Bubble formation at an orifice in an invisid liquid, *Trans. Inst. Chem. Engrs* **38**, 335–342 (1960).
17. J. K. Walters and J. F. Davidson, The initial motion of a gas bubble formed in an invisid liquid. Part 2. The three-dimensional bubble and the toroidal bubble, *J. Fluid Mech.* **17**, 321–336 (1963).
18. H. J. Ivey, Relationship between bubble frequency, departure diameter and rise velocity in nucleate boiling, *Int. J. Heat Mass Transfer* **10**, 1023–1040 (1967).
19. D. P. Jordan, Film and transition boiling, in *Advances in Heat Transfer* (edited by T. F. Irvine, Jr. and J. P. Hartnett), Vol. 5, pp. 109–115. Academic Press, New York (1968).
20. V. Sernas, J. H. Lienhard and V. K. Dhir, The Taylor wave configuration during boiling from a flat plate, *Int. J. Heat Mass Transfer* **16**, 1820–1821 (1973).
21. Y. Katto and K. Kikuchi, Study of forces acting on a heated surface in nucleate boiling at high heat fluxes, *Heat Transfer – Japan. Res.* **1**(3), 34–46 (1972).
22. Y. Katto and M. Kunihiro, Study of the mechanism of burn-out in boiling system of high burn-out heat flux, *Bull. JSME* **16**, 1357–1366 (1973).
23. Y. Katto and S. Yokoya, Principal mechanism of boiling crisis in pool boiling, *Int. J. Heat Mass Transfer* **11**, 993–1002 (1968).
24. Y. Katto, S. Yokoya and M. Yasunaka, Mechanism of boiling crisis and transition boiling, *Proc. 4th Int. Heat Transfer Conf.* Paris, vol. V, B3.2 (1970).
25. Y. Katto and C. Kurata, Critical heat flux of saturated convective boiling on uniformly heated plates in a parallel flow, *Int. J. Multiphase Flow* **6**, 575–582 (1980).
26. G. C. Vliet and G. Leppert, Critical heat flux for nearly saturated water flowing normal to a cylinder, *Trans. Am. Soc. Mech. Engrs*, Series C, *J. Heat Transfer* **86**, 59–67 (1964).
27. G. C. Vliet and G. Leppert, Critical heat flux for subcooled water flowing normal to a cylinder, *Trans. Am. Soc. Mech. Engrs*, Series C, *J. Heat Transfer* **86**, 68–74 (1964).
28. S. Yilmaz and J. W. Westwater, Effect of velocity on heat transfer to boiling Freon-113, *Trans. Am. Soc. Mech. Engrs*, Series C, *J. Heat Transfer* **102**, 26–31 (1980).
29. N. Zuber, Nucleate boiling. The region of isolated bubbles and the similarity with natural convection, *Int. J. Heat Mass Transfer* **6**, 53–78 (1963).

UN NOUVEAU MODELE HYDRODYNAMIQUE DU FLUX THERMIQUE CRITIQUE APPLICABLE LARGEMENT A L'EBULLITION EN RESERVOIR ET A L'EBULLITION FORCEE SUR DES CORPS IMMERGES DANS LES LIQUIDES SATURES

Résumé—Une instabilité d'Helmholtz est imposée sur l'interface vapeur–liquide des colonnes de vapeur distribuées dans une couche liquide mouillant une surface chauffée. Ce système vapeur–liquide est collapsé complétement par l'instabilité, mais à cause de la suppression de la surface solide, un film liquide mince incluant les troncs de vapeur part de la surface avec une certaine épaisseur définite en relation avec la longueur d'onde critique de Helmholtz. Une couverture de vapeur formée sur le film liquide restreint l'alimentation en liquide par le coeur du film, ce qui provoque la disparition du liquide sur la surface chaude et l'apparition du flux critique (CHF). Basé sur ce concept, un nouveau modèle hydrodynamique est développé et le CHF dans les systèmes d'ébullition fondamentaux sont représentés non seulement pour l'ébullition en réservoir mais aussi pour l'ébullition en convection forcée, ce qui suggère la validité de la signification physique du modèle.

EIN NEUES HYDRODYNAMISCHES MODELL DER KRITISCHEN WÄRMESTROMDICHTE FÜR EINEN WEITEN BEREICH DES BEHÄLTER- UND STRÖMUNGS-SIEDENS AN KÖRPERN IN GESÄTTIGTER FLÜSSIGKEIT

Zusammenfassung—In diesem Aufsatz wird die Helmholtz-Instabilität auf die Dampf-Flüssigkeits-Grenzfläche von Dampfsäulen angewandt, die in der Flüssigkeitsschicht verteilt sind, welche eine beheizte Oberfläche benetzt. Das Dampf-Flüssigkeits-System ist durch die Instabilität vollständig zusammengebrochen, aber infolge der dämpfenden Wirkung der festen Oberfläche bleibt ein dünner Flüssigkeitsfilm, der Dampfsäulen enthält, stabil auf der Oberfläche erhalten. Er besitzt eine bestimmte Dicke entsprechend der kritischen Helmholtz-Wellenlänge. Eine Dampf-Decke, die sich über dem Flüssigkeitsfilm ausbreitet, verhindert die Flüssigkeitszufuhr vom Kerngebiet zum Film mit dem Ergebnis, daß die Flüssigkeit von der beheizten Oberfläche verschwindet. Dies ist das Auftreten der kritischen Wärmestromdichte. Auf der Grundlage des vorgenannten Konzepts wird ein neues hydrodynamisches Modell entwickelt. In analytischen Untersuchungen wird die kritische Wärmestromdichte in fundamentalen Siedesystemen veranschaulicht, und zwar sowohl beim Behälter- als auch beim Strömungssieden, was die Gültigkeit der physikalischen Struktur dieses Modells bestätigt.

НОВАЯ ГИДРОДИНАМИЧЕСКАЯ МОДЕЛЬ КРИТИЧЕСКОГО ТЕПЛОВОГО ПОТОКА, ПРИГОДНАЯ ДЛЯ ОПИСАНИЯ КИПЕНИЯ КАК В БОЛЬШОМ ОБЪЕМЕ, ТАК И ПРИ ВЫНУЖДЕННОЙ КОНВЕКЦИИ В СЛУЧАЕ ТЕЛ, ПОГРУЖЕННЫХ В НАСЫЩЕННУЮ ЖИДКОСТЬ

Аннотация—В настоящей работе условия устойчиваости Гельмгольца налагаются на границу раздела фаз пар-жидкость в стволах пара, распределенных в слое жидкости, смачивающем нагретую поверхность. Распад такой парожидкостной системы происходит исключительно за счет неустойчивости, однако на твердой поверхности остается тонкая пленка жидкости, включающая в себя стволы пара, толщина которой составляет некоторую величину, соответствующую критической длине волны Гельмгольца. Паровое покрывало, образованное таким образом на пленке жидкости, ограничивает подачу жидкости из основного объема на пленку, в результате чего жидкость исчезает с нагретой поверхности, что соответствует критическому тепловому потоку (КТП). На основании вышеизложенного разработана новая гидродинамическая модель, а анализ КТП иллюстрируется примерами не только для кипения в большом объеме, но и для кипения с вынужденной конвекцией, что позволяет говорить о правильности физической структуры данной модели.